RSC Advances

PAPER

View Article Online
View Journal | View Issue

Cite this: *RSC Adv.*, 2016, **6**, 62445

Mg_9Si_5: a potential non-toxic thermoelectric material for mid-temperature applications†

Vijeta Singh,[a] J. J. Pulikkotil[abc] and S. Auluck*[c]

Received 1st April 2016
Accepted 13th June 2016

DOI: 10.1039/c6ra08389g

www.rsc.org/advances

Mid-temperature thermoelectric applications include waste heat recovery from automobile exhausts, various industrial process and solar thermoelectrics. The current systems that have been extensively investigated for mid-temperature applications are mostly tellurides. However, the low crustal abundance of tellurium contributes significantly to their price volatility which impedes their usage in commercial technology. Looking from the perspective of material cost effectiveness in terms of crustal abundance and environmental sustainability, we investigate the thermoelectric properties of Mg_9Si_5 systems, the constituents of which are geo-abundant and non-toxic. By means of first principles calculations, we find Mg_9Si_5 to be a potential mid-temperature thermoelectric material, with an operational temperature in the range of $\simeq$400–600 K, depending on the exact carrier concentration. We also discuss the enhanced viability of substitution in Mg_9Si_5, a case that seems to be restricted in Mg_2Si because of its chemically balanced Zintl nature.

1 Introduction

One of the solid state solutions to the increasing global energy demand lies in the commercialization of thermoelectric materials. These materials, by means of the Seebeck effect, help in converting heat into useful electrical energy. In terms of its operation and efficiency, a thermoelectric material is judged on its figure of merit (zT).[1] However, what often impedes the optimization of materials towards higher zT values is the strong interdependence of transport parameters, namely electrical conductivity (σ), Seebeck coefficient (S) and thermal conductivity (κ). Nevertheless, experimental observations and theoretical models have significantly contributed to a better understanding of thermoelectric material design and modelling. Enhancement of the thermoelectric performance of materials has been significantly optimized by fine tuning growth parameters and synthesis conditions thereby controlling carrier concentration. This has also been accomplished by appropriate chemical doping, nanostructuring[2–5] and other state-of-the-art techniques. In part these techniques have brought thermoelectric material optimization closer to the realization of a "phonon-glass electron-crystal", as originally proposed by Slack.[6]

On the other hand, a few empirical criteria that help towards the design of such materials are high symmetry structures, in which multiple valleys in their band structure can improve the electronic contribution to zT. Large unit cell systems with their constituents having different masses are also beneficial, as such systems help in reducing thermal conductivity *via* phonon scattering. Besides, the Pisarenko plot of thermoelectric transport parameters suggests that the most promising materials are narrow band gap semiconductors.[7]

Genuine interest may lie in optimizing Si–Ge alloys for mid-temperature applications by band gap engineering.[8–10] A ternary substituent, such as Sn, is expected to decrease the band gap, thereby lowering its operational temperature to the mid-temperature range.[11] However, what impedes the design of such materials is the solubility of the substituent in the SiGe host matrix. Another class that is promising for mid-temperature applications is Mg–Si binary systems.[12–16] For instance, Mg_2Si which crystallizes in an anti-fluorite cubic structure is an environmentally friendly material, besides its constituent elements being abundant in the earth's crust.[17,18] Intrinsic Mg_2Si shows n-type conduction with a carrier concentration as low as 10^{17} cm^{-3} at 300 K. However, with appropriate chemical doping the carrier concentration could be enhanced to $\sim 10^{19}$ cm^{-3}.[19] The thermal conductivity also decreases with increasing temperature with its lattice contribution being predominant. For an n-type thermoelectric device based on Mg_2Si, the zT of the material has been optimized to 1.4,[20,21] while for p-type a zT of 0.7 has been achieved.[21,22] The primitive unit cell of Mg_2Si contains 12 atoms, with 4 Si ions in the first coordination shell of each Mg ion and 8 Mg ions in the first coordination shell of Si. We note that a large average

[a]*Academy of Scientific & Innovative Research (AcSIR), CSIR-National Physical Laboratory, New Delhi, India*

[b]*Computational and Network Facility, CSIR-National Physical Laboratory, New Delhi, India*

[c]*Quantum Phenomenon and Applications Division, CSIR-National Physical Laboratory, New Delhi, India. E-mail: sauluck@iitk.ac.in*

† Electronic supplementary information (ESI) available. See DOI: 10.1039/c6ra08389g

coordination number per ion is quite beneficial for reducing the phonon mean free path, thereby reducing the lattice thermal conductivity.[23,24] Furthermore, the presence of large voids in the Mg_2Si structure not only softens the lattice,[25] but also provides enough space for the ions to rattle, thereby leading to enhanced phonon scattering in these systems. In fact, Mg_2Si falls in the category of a Zintl phase, where a strong electropositive element such as Mg donates its valence electrons to a covalent Si–Si network; the latter provides a pathway for electrical conduction in the system. However, it is also this electrochemical balance which impedes carrier concentration tuning in the system *via* chemical substitution. Various elemental substitutions such as Al,[26,27] Pb,[28] Bi[29] and Ag[30,31] have been reported. However their solubility limit does not exceed more that 0.2–0.3 at% in Mg_2Si.

Recently, a new compound with the generic formula Mg_9Si_5 has been reported in the Mg–Si phase diagram, which is synthesized under high pressure. Mg_9Si_5 crystallizes in a hexagonal symmetry, with 54 Mg atoms and 30 Si atoms in the unit cell.[38] The fraction of volume that is occupied by Mg and Si in Mg_9Si_5 (*i.e.*, the packing fraction) is estimated to be $\simeq$45%, while in Mg_2Si this fraction corresponds to $\simeq$50%. The presence of large voids in Mg_9Si_5 are therefore indicative of a softer underlying lattice. Such lattices are anticipated to dampen phonon propagation in the system. In addition, structural refinements also show a large variance in Mg–Si and Si–Si bond lengths, which introduces bond disorder. Besides, unlike the stoichiometric Mg_2Si, the charge balance in Mg_9Si_5 is stabilized *via* a strongly knit covalent Si network. As mentioned above, these structural features are quite preferable in thermoelectric material design, which would significantly reduce lattice thermal conductivity. Therefore, deducing from its structural features that Mg_9Si_5 has favorable thermoelectric properties, we studied the electronic structure and transport properties of the system, by means of *ab initio* density functional theory calculations. Our full potential calculations, based on the linearized augmented plane wave method, show that Mg_9Si_5 is a narrow band semiconductor with a band gap of $\simeq$0.2 eV, which is approximately one third that of Mg_2Si ($\simeq$0.6 eV).[32] On a phenomenological level, we therefore argue that the material's optimized thermoelectric performance can be tuned in the range 400–800 K, depending on the exact carrier concentration in the system.

2 Computational details

Calculations were performed using the linearized augmented plane-wave (LAPW) method[33] as implemented in the WIEN2K suite of program code.[34] The equilibrium lattice constants were taken from experiments and the internal coordinates of the Mg and Si ions were fully relaxed by force optimization methods. The exchange–correlation term of the Kohn–Sham Hamiltonian were described using the generalized gradient approximation (GGA) of Perdew, Burke, and Ernzerhof.[35] The Brillouin zone was sampled with a k-mesh of 15 × 15 × 13 in the irreducible wedge for the total energy calculations amounting to 273 k-points. A much denser grid of size 48 × 48 × 42 k-mesh, totalling 8492 irreducible k-points, was used for the transport calculations. Well-converged basis sets with $R_{MT}K_{max} = 7$, with R_{MT} and K_{max} being the smallest muffin-tin radius and the maximum size of reciprocal lattice vectors, respectively, were used. The LAPW sphere radii for Mg and Si ions were $2.5a_0$ and $2.24a_0$, with a_0 being defined as the Bohr radius. The core electrons were treated relativistically, and relativistic effects were included at the scalar relativistic level for the valence electrons. Based on our experience that GGA underestimates the band gap of Mg_2Si and that a better solution consistent with experiments could be derived from the modified Becke–Johnson potential, we extended our calculations for Mg_9Si_5 in much a similar way. We note that the recently developed mBJ functional[41] by Tran and Blaha that accounts for exchange–correlation in solids significantly improves the band gap of many semiconductors. The Mg–Si binary systems appear to be one class accounting for the success of the mBJ method without any adjustable parameters.

Transport properties were calculated from the electronic structure using Boltzmann theory and the constant scattering time approximation (CSTA) as implemented in the BoltzTraP code.[36] The CSTA, which has been successfully applied to a wide range of thermoelectric materials[37] allows the direct calculation of Seebeck coefficient as a function of temperature and doping level, with no adjustable parameters.

3 Results and discussions

3.1 Structural optimization

To substantiate, from structural considerations, that Mg_9Si_5 would have a low thermal conductivity, we first analyze the structural details obtained from the fully relaxed GGA calculations. Mg_9Si_5 crystallizes in a hexagonal $P6_3$ symmetry with its unit cell consisting of 84 atoms in total. As we can see from Fig. 1, there are 54 Mg atoms distributed onto 9 inequivalent 6c sites, and 30 Si atoms distributed onto 2a, 2b and 6c sites. For a detailed description of the structure, we refer to ref. 38. With the atomic coordinates of all Mg ions in the systems not fixed by symmetry and also the z-coordinates of all Si ions, the arrangement of the atoms in an underlying hexagonal symmetry gives a different local environment for each Si atom. Within a 3 Å local coordination shell, the immediate local

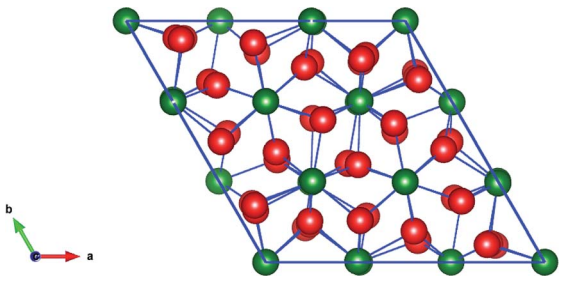

Fig. 1 Schematic illustration of the crystal structure of the hexagonal Mg_9Si_5 along the crystallographic c-axis where Mg and Si atoms are shown by red and green spheres respectively. Mg atoms are distributed onto 9 inequivalent 6c sites and Si atoms are distributed onto 2a, 2b and 6c sites.

neighbourhood of a Si(2a) site is composed of 1 Si atom and 3 Mg ions, while a Si(2b) site has 1 Si ion and 6 Mg ions. The Si(6c) sites are coordinated by 9 Mg ions within a coordination shell of 3 Å radius. GGA optimization of structural parameters shows that the nearest Si(2a)–Mg(6c) bond distance average is 2.713 ± 0.057 Å, that of Si(2b)–Mg(6c) is 2.794 ± 0.128 Å and that of Si(6c)–Mg(6c) is 2.804 ± 0.077 Å. Thus, on a phenomenological basis, we infer that such large deviations in the bond distances between similar ionic pairs serves as potential cause of scattering for phonon propagation in the material, which would lower the lattice thermal conductivity.[39,40] On the other hand the near neighbor Si(2a)–Si(2a) and Si(2b)–Si(2b) bond distances were estimated to be 2.509 and 2.496 Å, respectively. These Si–Si pairs are substantially shorter than the Si–Mg pairs and serve as an electron conduction pathway in the system.

3.2 Electronic structure

In the PBE-GGA calculation scheme, we find Mg_9Si_5 to be a metal. We note that by a similar approximation, although Mg_2Si was predicted to be a semiconductor the magnitude of the band gap was severely underestimated.[32] The PBE-GGA also incorrectly predicts Mg_2Sn to be a metal. It is well known that GGA generally underestimates the band gap, a feature inherent to the approximation. However, improved results could be realized with the recently proposed exchange–correlation potential by Tran and Blaha, otherwise known as the modified Becke–Johnson potential.[41] In Fig. 2 we show the total and atom resolved densities of states of Mg_9Si_5 calculated using the mBJ-GGA scheme. It is evident that the Mg and Si states are distributed over a wide energy range, showing covalent interaction in the system. The near Fermi energy is dominated by Si 3p states, with little admixture of Mg 3s states. In the mBJ-GGA calculations, an electronic gap of magnitude 0.17 eV was calculated for Mg_9Si_5, which is comparable with that of Bi_2Te_3 (0.15 eV)[47] and Bi_2Se_3 (0.24 eV).[48] The magnitude of band gap suggests that Mg_9Si_5 could be a potential near-room temperature thermoelectric, having additional advantages over the tellurides in terms of eco-friendliness and material abundance. Hereby, we note that we are unaware of any transport data, with which the predicted band gap of Mg_9Si_5 using the mBJ-GGA potential could be compared with. However, given that the approximation yields results for Mg_2Si that are very consistent with experiments, the predicted value may well be thought to be reliable.

A closer inspection of the DOS spectra in terms of the site decomposed Si atoms, as shown in Fig. 3, reveals that the gap structure is essentially between that of the atoms residing at the 6c position. On the other hand, the DOS emanating from the Si(2a) and Si(2b) states across the E_F appears nearly degenerate. An electronic gap, almost twice as large, is observed between these Si(2a) and (2b) states, which amounts to $\simeq$0.32 eV. In consideration with the local environment of the Si atoms at the 2a, 2b and 6c positions, it may be therefore inferred that the nature of the electronic gap in Mg_9Si_5 is hybridization driven. The Si(2a) and Si(2b) atom forms strong covalent dimers in this system, while the Si(6c) atoms are surrounded by strong electropositive Mg ions.

In Fig. 4, we show the *k*-resolved energy spectrum of Mg_9Si_5. As is evident from the band structure, Mg_9Si_5 manifests itself as a indirect band gap semiconductor, *i.e.*, the valence band maximum is at the Γ-point while the conduction band minimum is at the *M* point of the hexagonal Brillouin zone. The direct band gaps along the Γ and *M* points are 0.35 eV and 0.37 eV, respectively. We note that the band dispersion along Γ–*A* is representative of the interactions between the atoms in the basal *a*–*b* plane of the hexagonal unit cell in real space, while Γ–*M* manifests the interactions along the *c*-axis of the unit-cell. The dispersion of the bands in the valence band region along Γ–*M* and Γ–*A* are quite different. Those along Γ–*A* are strongly dispersed, while that along Γ–*M* are nearly flat around the Γ point. The very different dispersion of the Si 3p states along the

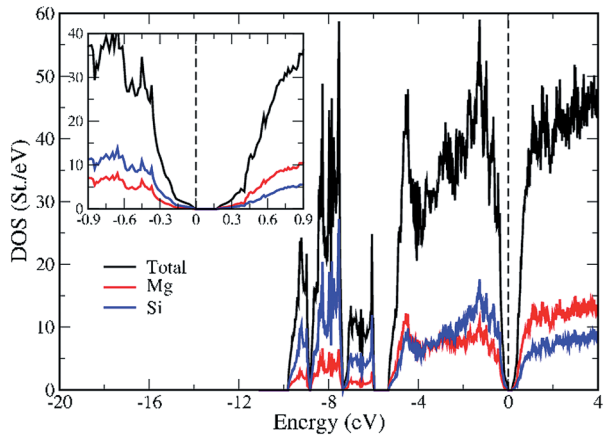

Fig. 2 The total (black curve) and atom resolved Mg (red curve) and Si (blue curve) partial densities of states of Mg_9Si_5 calculated using mBJ-GGA. The vertical line through zero energy represents the reference Fermi energy. The inset shows a blow-up of the region around the Fermi energy.

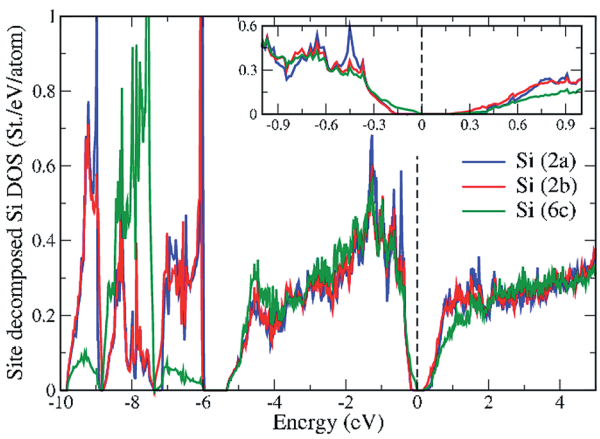

Fig. 3 The site decomposed Si partial density of states computed by means of mBJ-GGA calculations, with the Si(2a), (2b) and (6c) contributions shown by blue, red and green curves. The vertical line through zero energy represents the reference Fermi energy and, the inset shows a blow-up of the region around the Fermi energy.

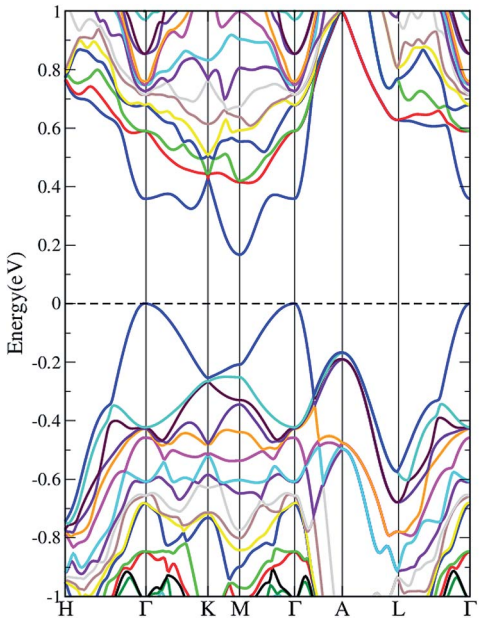

Fig. 4 The mBJ-GGA generated k-resolved band structure of Mg_9Si_5. The horizontal line through zero energy represents the reference Fermi energy.

Γ–A and Γ–M directions indicates anisotropy in the transport properties of Mg_9Si_5.

According to Mott's equation[42] the performance of a thermoelectric material depends on the density of states effective mass (m_b^*). In the regime where the carriers are scattered mainly by acoustic phonons, the most commonly accepted relation is $\mu \propto (m_b^*)^{-3/2} m_c^{*-1}$ where μ is the carrier mobility[43] and m_c^* the conduction mass of the carriers. However, the optimal electronic performance of a thermoelectric material depends primarily on the weighted mobility, given by $\mu m^{*-3/2}$.[44–46] Thus, to optimize both effects, a combination of heavy and light bands would be crucial to optimize the electronic performance of a thermoelectric system. In Mg_9Si_5, we observe such a scenario in its band structure. As discussed above, the top of the valence band is composed of heavy bands along $\tilde{A}$–M and light bands along the $\tilde{A}$–A, $\tilde{A}$–L and $\tilde{A}$–H directions.

3.3 Transport properties

In Fig. 5 and 6, we show Pisarenko plots comparing Seebeck coefficient (S) as a function of carrier concentration, for both p-type and n-type charge carriers, respectively. It is in fact a general rule that in doped semiconductors and metals, the Seebeck coefficient varies inversely proportionally to carrier concentration.[7] As is evident from Fig. 5(a) and 6(a), a very similar relation between $S(T)$ and $n_e(n_p)$, for a given temperature is also observed in Mg_9Si_5. However, the variation is quite different for both p-type and n-type charge carriers. In the case of p-type doping the peak maximum of S remains more or less constant ($\simeq$230 $\mu V\ K^{-1}$), and shifts to higher carrier concentration with increasing T. However, for n-type dopants, the peak maximum steadily decreases with both increasing carrier

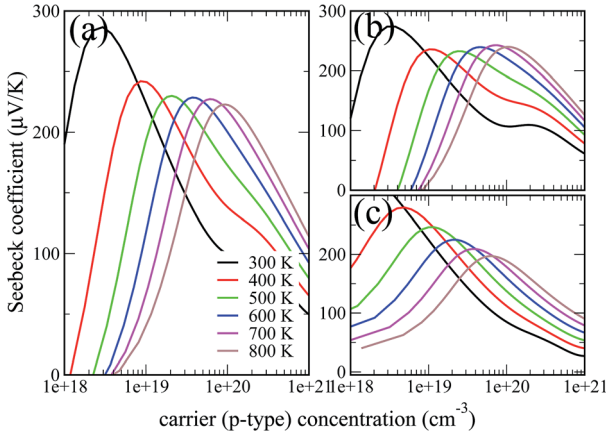

Fig. 5 Pisarenko plot showing the variation of Seebeck coefficient as a function of p-type carrier concentration in Mg_9Si_5, calculated using the Boltzmann transport equation in the constant relaxation time approximation. In panel (a) is shown the averaged Seebeck coefficient evaluated as $(2S_{xx} + S_{zz})/3$; $S_{xx} \equiv S_{yy}$, where $S_{xx}(S_{yy})$ represent the in-plane contribution to the Seebeck tensor and S_{zz} the out-of-plane component. Panels (b) and (c) represent S_{xx} and S_{zz}, respectively.

concentration and T. This more or less reflects the asymmetry of the band dispersion across the electronic gap in the system. Here we note in estimating the effects of $S(T)$ on carrier concentration, the $n_e(n_p)$ has been calculated *via* a rigid band shift in the materials E_F.

In Fig. 5(b) and (c) and in Fig. 6(b) and (c), we show the variation in the in-plane ($S_{xx(yy)}$) and out-of-plane S_{zz} contribution to the average S, as a function of p and n-type carrier concentration in Mg_9Si_5. Note that the hexagonal symmetry of Mg_9Si_5 implies that the Seebeck tensor elements will be diagonal and that the $S_{xx(yy)}$ and S_{zz} components would be different. For p-type carriers, the variation in $S_{xx}(T)$ with n shows more or

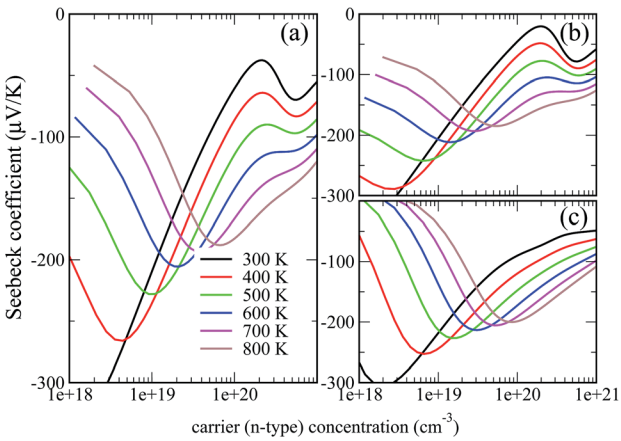

Fig. 6 Pisarenko plot showing the variation of Seebeck coefficient as a function of n-type carrier concentration in Mg_9Si_5, calculated using the Boltzmann transport equation in the constant relaxation time approximation. In panel (a) is shown the averaged Seebeck coefficient evaluated as $(2S_{xx}+S_{zz})/3$; $S_{xx} \equiv S_{yy}$, where $S_{xx}(S_{yy})$ represent the in-plane contribution to the Seebeck tensor and S_{zz} the out-of-plane component. Panels (b) and (c) represent S_{xx} and S_{zz}, respectively.

less a shift of the peak maximum towards higher n_p values, while the magnitude of the $S_{zz}(T)$ decreases steadily. In the case of n-type carriers in Mg_9Si_5 the peak maxima associated with the $S_{xx}(T)$ and $S_{zz}(T)$ decreases steadily. The anisotropy in the Seebeck coefficient, *i.e.*, $S_{xx(yy)}/S_{zz}$, calculated for p-type carriers for $n_p = 2 \times 10^{19}$ at $T = 600$ K is estimated as 0.96, while the corresponding value for the case of n-type carriers is estimated as 1.10. The rather small deviation in the calculated S values along the c-axis and in-plane refers Mg_9Si_5 as a three dimensional material.

In Fig. 7 and 8, we show the temperature dependent variation of S for a few selected carrier concentrations. It is also observed that the S_{max} can be tuned to the range 400–800 K, depending on the exact carrier concentration in the system. For instance, S_{max} for $n_e(n_p) = 2 \times 10^{19}$ cm^{-3} is calculated to be 205 μV K^{-1} (230 μV K^{-1}), while for $n_e(n_p) = 8 \times 10^{19}$ it is determined as 195 μV K^{-1} (225 μV K^{-1}). In order to compare the transport coefficients more directly to thermoelectric behavior, it is useful to rewrite the figure of merit $ZT = s\nu S^2 T/(\kappa_l + \kappa_e) = rS^2/L$, where $r = \kappa_e/(\kappa_l + \kappa_e)$ and $L = \kappa_e/(s\nu T)$, *i.e.*, the Lorenz number in the Wiedemann–Franz relation. The fact that one must have $r \leq 1$ implies that the value of thermopower sets an upper bound on ZT. Lattice thermal conductivity is not known for the system so from the argument in ref. 32 for Mg_2Si, it is clear that with the standard value of $L = L_0$, $r = 0.5$, and $S = 250$ mV K^{-1} this formula gives $ZT \sim 1.3$. Finally, this formula shows the importance of lattice thermal conductivity in setting the scale of the ZT achievable. Our Seebeck coefficient is 15% less than the value for Mg_2Si. In the absence of any experimental thermal conductivity value of Mg_9Si_5 we assume the same thermal conductivity of Mg_2Si. This gives a ZT value of ~1. We expect Mg_9Si_5 to have a smaller thermal conductivity than Mg_2Si resulting in a larger ZT value. With S being an important parameter in optimizing the thermoelectric figure of merit, as it enters the zT equation quadratically, the broad maximum in S_{max} as well as the temperature range, manifests that Mg_9Si_5 is a potential thermoelectric material in the mid-temperature range.

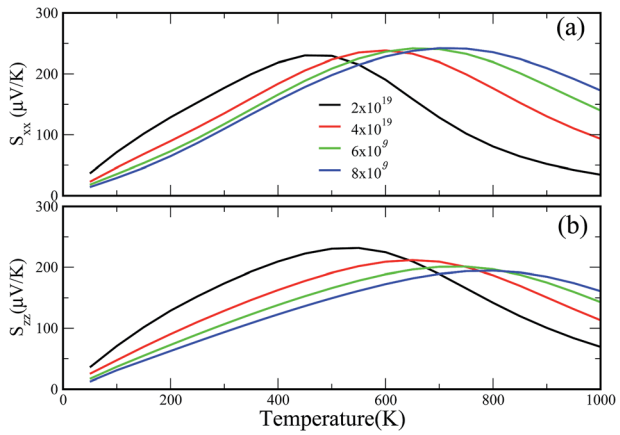

Fig. 7 The calculated variation of Seebeck coefficient (S) in Mg_9Si_5 as a function of temperature for various electron charge concentration for p-type carriers, as indicated. (a) The *xx* component of the Seebeck coefficient tensor representing the in-plane contribution and (b) the *zz* component, representing the Seebeck coefficient along the crystallographic c-axis. Here, S is expressed in units of mV K^{-1}.

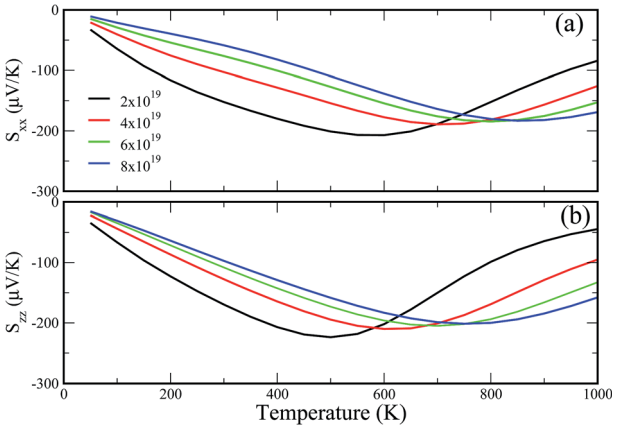

Fig. 8 The calculated variation of Seebeck coefficient (S) in Mg_9Si_5 as a function of temperature for various electron charge concentration for n-type carriers, as indicated. (a) The *xx* components of the Seebeck coefficient tensor representing the in-plane contribution and (b) the *zz* component, representing the Seebeck coefficient along the crystallographic c-axis. Here, S is expressed in units of mV K^{-1}.

4 Summary and conclusion

In summary, using first principles density functional theory based calculations, using the mBJ-GGA potential to describe the exchange correlations effects, we find that Mg_9Si_5 is a potential non-toxic mid temperature thermoelectric material, operable in the 400–600 K range. The magnitude of the electronic band gap of 0.17 eV and the density of states spectra in the vicinity of E_F show the strong domination of the Si 3p states. With a large number of atoms and varying bond lengths between similar constituents in the system, we argue from a phenomenological point of view that the thermal conductivity of the system would be much lower that its Mg_2Si counterpart. However, we note that there exists an upper limit to thermoelectric performance, as beyond $\simeq$700 K, Mg_9Si_5 transforms to Mg_2Si which is an irreversible structural reaction. Hence, the operational range of Mg_9Si_5 is rather restricted to 400–600 K. Further, it is also shown in the experiments that carrier tuning can be achieved using Al at the Mg site for the n-type material.

Acknowledgements

V. S. thanks the Council of Scientific and Industrial Research (CSIR)–National Physical Laboratory for financial support and JJP acknowledges funding from the CSIR-XIIth five year plan project AQuaRIUS. SA would like to acknowledge use of the computing facilities at IUAC (Intra-University Accelerator Centre, New Delhi), IMSC (Institute of Mathematical Sciences, Chennai) and IITK (Indian Institute of Technology, Kanpur). The authors gratefully acknowledge the use of CSIR High

Performance Computing Facilities at CSIR-4PI, Bangalore, India for this research.

References

1 The figure-of-merit (zT) of a thermoelectric material is mathematically defined as $zT \equiv (\sigma^2 S/\kappa)T$ where σ is the electrical conductivity, S the Seebeck coefficient and κ the thermal conductivity.
2 K. Biswas, J. He, Q. Zhang, G. Wang, C. Uher, V. P. Dravid and M. G. Kanatzidis, *Nat. Chem.*, 2011, **3**(2), 160.
3 P. F. Poudeu, J. D'Angelo, A. D. Downey, J. L. Short, T. P. Hogan and M. G. Kanatzidis, *Angew. Chem.*, 2006, **118**(23), 3919.
4 Y. Pei, J. Lenscha-Falk, E. S. Toberer, L. Douglas, D. L. Medlin and G. J. Snyder, *Adv. Funct. Mater.*, 2011, **21**(2), 241.
5 M. G. Kanatzidis, *Chem. Mater.*, 2009, **22**(3), 648.
6 G. A. Slack, in *CRC Handbook of Thermoelectronics*, ed. D. M. Rowe, CRC Press, Boca Raton, FL, 1995, p. 407.
7 A. F. Ioffe, *Physics of Semiconductors*, Academic Press Inc., New York1960.
8 S. Bathula, M. Jayasimhadri, N. Singh, A. K. Srivastava, J. Pulikkotil, A. Dhar and R. C. Budhani, *Appl. Phys. Lett.*, 2012, **101**(21), 213902.
9 X. W. Wang, H. Lee, Y. C. Lan, G. H. Zhu, G. Joshi, D. Z. Wang and S. Song, *Appl. Phys. Lett.*, 2008, **93**(19), 193121.
10 R. Basu, S. Bhattacharya, R. Bhatt, M. Roy, S. Ahmad, A. Singh and S. K. Gupta, *J. Mater. Chem. A*, 2014, **2**(19), 6922–6930.
11 J. J. Pulikkotil and S. Auluck, *AIP Adv.*, 2015, **5**(3), 037145.
12 C. R. Whitsett and G. C. Danielson, *Phys. Rev.*, 1955, **100**(4), 1261–1262.
13 R. G. Morris, R. D. Redin and G. C. Danielson, *Phys. Rev.*, 1958, **109**(6), 1909.
14 R. J. LaBotz, D. R. Mason and D. F. Okane, *J. Electrochem. Soc.*, 1963, **110**(2), 127.
15 P. M. Lee, *Phys. Rev.*, 1964, **1359**(4A), A1110.
16 T. C. Harman, P. J. Taylor, D. L. Spears and M. P. Walsh, *J. Electron. Mater.*, 2000, **29**, L1.
17 T. Caillat, A. Borshchevsky and J. P. Fleurial, *J. Appl. Phys.*, 1996, **80**, 4442.
18 S. Bose, H. N. Acharya and H. D. Banerjee, *J. Mater. Sci.*, 1993, **28**, 5461.
19 W. Wunderlich, Y. Suzuki, N. Gibo, T. Ohkuma, M. Al-Abandi, M. Sato, A. U. Khan and T. Mori, *Inorganics*, 2014, **2**(2), 351.
20 W. Liu, X. Tang, H. Li, K. Yin, J. Sharp, X. Zhou and C. Uher, *J. Mater. Chem.*, 2012, **22**(27), 13653.
21 W. Liu, Q. Zhang, K. Yin, H. Chi, X. Zhou, X. Tang and C. Uher, *J. Solid State Chem.*, 2013, **203**, 333.
22 T. Sakamoto, T. Iida, A. Matsumoto, Y. Honda, T. Nemoto, J. Sato, T. Nakajima, H. Taguchi and Y. Takanashi, *J. Electron.Mater.*, 2010, **39**(9), 1708.
23 G. J. Snyder and E. S. Toberer, *Nat. Mater.*, 2008, **7**(2), 105–114.
24 Y. S. Ju and K. E. Goodson, *Appl. Phys. Lett.*, 1999, **74**(20), 3005–3007, respectively.
25 J. J. Pulikkotil, H. N. Alshareef and U. Schwingenschlogl, *J. Phys.: Condens. Matter*, 2010, **22**(35), 352204.
26 S. Battiston, S. Fiameni, M. Saleemi, S. Boldrini, A. Famengo, F. Agresti and S. Barison, *J. Electron. Mater.*, 2013, **42**(7), 1956.
27 J. Tani and H. Kido, *Jpn. J. Appl. Phys.*, 2007, **46**(6), 3309.
28 S. Muthiah, J. Pulikkotil, A. K. Srivastava, A. Kumar, B. D. Pathak, A. Dhar and R. C. Budhani, *Appl. Phys. Lett.*, 2013, **103**(5), 053901.
29 J. I. Tani and H. Kido, *Phys. B*, 2005, **364**(1), 218.
30 M. Akasaka, T. Iida, A. Matsumoto, K. Yamanaka, Y. Takanashi, T. Imai and N. Hamada, *J. Appl. Phys.*, 2008, **104**(1), 013703.
31 J. Tani and H. Kido, *Intermetallics*, 2008, **16**(3), 418.
32 J. J. Pulikkotil, D. J. Singh, S. Auluck, M. Saravanan, D. K. Misra, A. Dhar and R. C. Budhani, *Phys. Rev. B: Condens. Matter Mater. Phys.*, 2012, **86**(15), 155204.
33 D. J. Singh and L. Nordstrom, *Planewaves, Pseudopotentials and the LAPW Method*, Springer, Berlin, 2nd edn, 2006.
34 P. Blaha, K. Schwarz, G. Madsen, D. Kvasnicka and J. Luitz, An Augmented Plane Wave + Local Orbitals Program for Calculating Crystal Properties, *WIEN2K*, Tech. Univ., Wien, Austria, 2001.
35 J. P. Perdew, K. Burke and M. Ernzerhof, *Phys. Rev. Lett.*, 1996, **77**(18), 3865.
36 G. K. H. Madsen and D. J. Singh, *Comput. Phys. Commun.*, 2006, **175**(1), 67.
37 D. J. Singh, *Sci. Adv. Mater.*, 2011, **3**(4), 561.
38 S. Ji, M. Imai, H. Zhu and S. Yamanaka, *Inorg. Chem.*, 2013, **52**(7), 3953.
39 B. Qiu and X. Ruan, *Phys. Rev. B: Condens. Matter Mater. Phys.*, 2009, **80**(16), 165203.
40 N. Mingo, *Phys. Rev. B: Condens. Matter Mater. Phys.*, 2003, **68**(11), 113308.
41 F. Tran and P. Blaha, *Phys. Rev. Lett.*, 2009, **102**(22), 226401.
42 N. F. Mott and H. Jones, *The Theory of the Properties of Metals and Alloys*, Dover Publication, New York, 1958.
43 J. Bardeen and W. Shockley, *Phys. Rev.*, 1950, **80**(1), 72.
44 R. P. Chasmar and R. Stratton, *Int. J. Electron.*, 1959, **7**(1), 52.
45 G. D. Mahan, in *Solid State Phys.*, ed. H. Ehrenreich and F. Spaepen, Academic Press Inc, San Diego, 1998, p. 81.
46 G. A. Slack, in *CRC handbook of thermoelectrics*, ed. D. M. Rowe, CRC Press, Boca Raton, Fla, 1995, p. 406.
47 P. Larson, *Phys. Rev. B: Condens. Matter Mater. Phys.*, 2003, **68**(15), 155121.
48 B. Pejova, I. Grozdanov and A. Tanusevski, *Mater. Chem. Phys.*, 2004, **83**(2), 245.

